This is a preprint, the final version is subject to change, of the American Mineralogist (MSA)
Cite as Authors (Year) Title. American Mineralogist, in press.
(DOI will not work until issue is live.) DOI: http://dx.doi.org/10.2138/am.2014.4575 

Revision 1

# Speciation of and D/H partitioning between fluids and melts in silicate - D-O-H-C-N systems determined *in-situ* at upper mantle temperatures, pressures, and redox conditions

B. O. Mysen [1], T. Tomita [2], E. Ohtani [2], and A. Suzuki [2]

[1] Geophysical Laboratory, Carnegie Instn. Washington, USA. [2] Dept. Earth Planet. Mater. Sci., Graduate School of Science, Tohoku University, JAPAN

**Abstract**

Speciation of D-O-H-C-N volatiles in alkali aluminosilicate melts and of silicate in D-O-H-C-N fluid has been determined *in-situ* to 800°C and > 2 GPa under reducing and oxidizing redox conditions by using an externally-heated hydrothermal diamond anvil cell with Raman spectroscopy as the structural probe. Reducing conditions were near those of the IW oxygen buffer, whereas oxidizing conditions were obtained by conducting the experiments with oxidized components only and with Pt as a catalyst.

Raman bands assigned to C-H stretching in $CH_xD_y$ isotopologues and $CH_4$ groups (including $CH_3$) were employed to determine the $CH_4/CH_xD_y$ ratio in fluids and melts. This ratio decreases from 1.5-2 at 500°C to between 1.2 and 1 with 800°C with $\Delta H$-values of 13.6±2.1 and 5.5±1.1 kJ/mol for melt and fluid, respectively. The $CH_4/CH_xD_y$ fluid/melt partition coefficient ranges between ~16 and ~3 with $\Delta H$=33±6 kJ/mol assuming no pressure effect. This behavior of deuterated and protonated complexes is ascribed to speciation of volatile and silicate components in fluids and melts in a manner that is conceptually similar to D/H partitioning among complexes and phases in brines and hydrous silicate systems.

Molecular $N_2$ is the N-bearing species in fluids and melts under oxidizing conditions. Under reducing conditions, the dominant species are molecular $NH_3$ and ammine groups, $NH_2^-$. The $NH_3/NH_2$ ratio varies between 0.15 and 0.75 in the 425°-800°C temperature range. The enthalpy change of the ammonia/ammine equilibrium, $\Delta H$, derived from the temperature and assuming no pressure effect on the equilibrium, is 19±8 kJ/mol and 61±9 kJ/mol for melt and fluid, respectively. The fluid/melt partition coefficient, $(NH_3 + NH_2^-)^{fluid}/(NH_3 + NH_2^-)^{melt}$, ranges from 8 to 3 with $\Delta H$=45±12 kJ/mol. For oxidized nitrogen, the fluid/melt partition coefficient is twice or more of

This is a preprint, the final version is subject to change, of the American Mineralogist (MSA)
Cite as Authors (Year) Title. American Mineralogist, in press.
(DOI will not work until issue is live.) DOI: http://dx.doi.org/10.2138/am.2014.4575 



those values for reduced nitrogen. Hydrogen bonding can be detected at 500°C and below. This behavior resembles that of $H_2O$. Deuterium-containing analogues of the (N+H)-species could not be detected with precision because these were in the frequency-range of the 2.-order Raman shift of diamond in the diamond anvil cell itself and could not be isolated from the strong background generated by the Raman intensity from the diamond.

## Introduction

Characterization of the processes that govern the budget and recycling of volatile components in the Earth's interior is central to our understanding of the formation and evolution of the solid Earth, its ocean and its atmosphere (e.g., Kasting et al., 1993; Tolstikhin and Marty, 1998; Cartigny and Ader, 2003; Kadik et al., 2013). The speciation and solubility of volatiles ($H_2O$, $CO_2$, CO, $CH_4$, $N_2$, $NH_3$, noble gases, etc.) in magmatic melts and fluids are integral parts of this understanding.

Oxygen fugacity affects the behavior of volatile-bearing magmatic systems because oxidized and reduced volatile species can behave quite differently (e.g., Saxena and Fei, 1987; Ulmer and Luth, 1991; Mysen et al., 2011). In the present silicate mantle $f_{O2}$ commonly is considered to be near redox conditions similar to QFM±1-2 (Wood et al., 1990; Luth et al., 1990; Canil, 2002). Under these conditions, the dominant C-O-H-N volatiles species are $H_2O$, $CO_2$, and $N_2$ with smaller amounts of $CH_4$ and $NH_3$ (Ulmer and Luth, 1991; Kasting et al., 1993; Holloway and Blank, 1994; Mysen et al., 2008, 2011). Under reducing conditions similar to those during the Earth's core-forming stage (perhaps 1-2 order of magnitude lower than that of the IW oxygen buffer) the main species were likely $CH_4$, $H_2O$, $H_2$, and $NH_3$ (Holland, 1984; Kasting et al., 1993; Mysen et al., 2011; Kadik et al., 2011). This redox-

This is a preprint, the final version is subject to change, of the American Mineralogist (MSA)
Cite as Authors (Year) Title. American Mineralogist, in press.
(DOI will not work until issue is live.) DOI: http://dx.doi.org/10.2138/am.2014.4575 



dependent speciation has profound effects because interaction between dissolved volatiles and the silicate melt solvent depends on their oxidation state. Melt properties vary with melt polymerization (for review, see for example, Mysen, 2012).

Most current experimental data on solubility and solution mechanisms of C-O-H-N volatiles in silicate melts are from analysis of glasses that were formed by quenching volatile-containing melts to ambient temperature at high pressure. Reliance on glass structure to establish melt structure/property relations requires that glass is, in fact, a quantitative proxy for melt. This is not the case because the glass structure records that of the liquid at its glass transition temperature. The glass transition temperature is hundreds of degrees lower than the liquidus temperature (Moynihan et al., 1976; Dingwell and Webb, 1990).

The C-O-H-N fluids in equilibrium with silicate at high temperature and pressure relevant to the deep crust and upper mantle cannot be quenched to ambient conditions for quantitative study because oxides dissolved in fluids commonly precipitate during quenching to ambient conditions. This is so because oxide solubility is greatly different at high temperature and pressure (Pascal and Anderson, 1989; Mysen and Armstrong, 2002; Kessel et al., 2004). It is very difficult, therefore, to extract compositional, isotopic, and structural information of high-temperature/-pressure fluids from examination of their quench products.

The experimental complications can be overcome by compositional and structural characterization of coexisting melts and fluids at the temperature and pressure of interest. This is the objective of the present report. Here, structure and D/H isotopic behavior of

This is a preprint, the final version is subject to change, of the American Mineralogist (MSA)
Cite as Authors (Year) Title. American Mineralogist, in press.
(DOI will not work until issue is live.) DOI: http://dx.doi.org/10.2138/am.2014.4575 



82 silicate - D-O-H-N-C fluids and melts in equilibrium in an externally-heated
83 hydrothermal diamond anvil cell have been determined *in-situ* by vibrational
84 spectroscopic methods with the samples at the desired high temperature, pressure, and
85 redox conditions.
86
87 **Experimental Methods**
88 The silicate starting material was the same $Na_2O$-$Al_2O_3$-$SiO_2$ NA10 glass {NA10:
89 $[(Na_2Si_4O_9)_{90}(Na_2(NaAl)_4O_9]_{10}$} as that used by Mysen (2007). In its molten form at
90 pressures less than that where Al- or Si-coordination transformation in aluminosilicate
91 melts occur, the degree of polymerization of NA10, expressed as NBO/T, is near 0.5. The
92 Al/(Al+Si) is near 0.2. In these respects, the composition resembles basaltic andesite. The
93 NA10 composition also is advantageous from a practical perspective because its liquidus
94 and glass transition temperatures are so low (Richet and Bottinga, 1984; Knoche et al.,
95 1994; Del Gaudio et al., 2007) that the melt is thermodynamically relaxed (supercooled
96 liquid) over a temperature interval of at least 500°C below the maximum sustainable
97 temperature in the Bassett diamond cell (≤1000°C; Bassett et al., 1996). These
98 circumstances provide a wide temperature interval over which to examine the interaction
99 of C-O-H-N volatile components with aluminosilicate melt.
100 Water was added as a $H_2O$:$D_2O$ mixture of 50 vol% of each component. We will
101 refer to this as water throughout this report. Nitrogen was added as $AgN_3$. The silver azide
102 decomposes to metallic Ag and $N_2$ below 350°C (Roskosz et al., 2006). Carbon was from
103 residue after cleaning of residual glue (Crystal Bond™ with acetone as cleaning agent)
104 employed during polishing of the gaskets before use.

This is a preprint, the final version is subject to change, of the American Mineralogist (MSA)
Cite as Authors (Year) Title. American Mineralogist, in press.
(DOI will not work until issue is live.) DOI: http://dx.doi.org/10.2138/am.2014.4575 



High-temperature/-pressure experiments were carried out in an externally-heated diamond anvil cell device (HDAC) (Bassett et al., 1994, 1996) with a 125 μm thick Ir gaskets with a 500 μm diameter central hole used for sample containment. During an experimental series, these dimensions shrunk to about 80 μm thickness in the region of contact with the 1-mm diamond culets and to a hole diameter near 400 μm. In the HDAC, external wire heaters surrounding each diamond aids in homogeneous temperature distribution (±2°C) over the entire sample.

The temperature was measured with two K-type thermocouples (in contact with the upper and lower diamonds) that are calibrated against the melting temperature of NaCl (800.5°C). Pressure was generated by the fluid because increasing temperature in a constant volume sample compartment increases the pressure. The presence of a C-O-H-N fluid phase also ensures hydrostatic pressure conditions. Pressure at high temperature was determined from the Raman shift of $^{13}C$ synthetic diamond (Bassett et al., 1996; Schiferl et al., 1997; Mysen and Yamashita, 2010). Spectrometer precision during the measurements of the $^{13}C$ diamond (±0.1 $cm^{-1}$) was optimized by using 2400 gratings/mm and Ne emission lines as internal frequency reference. The pressure/temperature effect on this Raman shift has been calibrated to an uncertainty of ±100 MPa with a ±40 MPa precision (Mysen and Yamashita, 2010). By combining this uncertainty with that of the Raman shift of the $^{13}C$ diamond at experimental conditions, overall pressure uncertainty of an experiment is ±110 MPa.

The experiments were carried out with two different redox conditions. Reducing conditions were obtained with the redox equilibrium, $Mo + H_2O = MoO_2 + H_2$, where Mo was added to the sample and was oxidized to $MoO_2$ via reaction of water at high

temperature and pressure. The $f_{O2}$ of this reaction in the presence of pure $H_2O$ is about an order of magnitude below that of the common redox buffer, Fe/FeO (iron-wustite). In mixed C-O-H-N fluids, the $f_{H2O}$ is less than for pure $H_2O$ thus leading to higher $f_{O2}$. Another series of experiments was carried out under what is referred to as "oxidizing conditions". In these experiments, small pieces of Pt metal was added to Mo-free starting materials. This Pt was employed to enhance isotope equilibration rate. There is no evidence that Pt reacts with water to form hydrogen and platinum oxide (Mysen, 2013a). The $f_{O2}$ was not buffered in these experiments.

*Structural Analysis*

Raman spectroscopy was used for structural examination. Spectroscopy was carried out with a JASCO model NRS-2000 microRaman spectrometer with a triple monochromator and a 400 mm focal distance. Spectra were recorded through a Mitutoyo 20X magnification/0.42 N.A. long-working distance objective lens. The samples were excited with the 488 nm line of a Spectra Physics, Stabilite 2017 Argon Ion Laser operating at 50 mW at the sample. A Princeton Instruments, LN/CCD-1100PF $LN_2$-cooled CCD is used for signal detection.

The measurements were conducted by subjecting a given sample in the HDAC to a series of temperatures and pressures. The sample was first brought to the highest temperature and pressure for a planned series of experiments (800˚C and 843 or 2165 MPa, for reduced and oxidized samples, respectively). After acquisition Raman spectra for carbon-13 diamond, fluid, and melt, the sample was brought to the next lower

This is a preprint, the final version is subject to change, of the American Mineralogist (MSA)
Cite as Authors (Year) Title. American Mineralogist, in press.
(DOI will not work until issue is live.) DOI: http://dx.doi.org/10.2138/am.2014.4575 



temperature. The temperature decrement per measurement was 75°C with 1°C/s cooling rate. Acquisition times ranged from 180 to 900 s/CCD window.

The spectra were first corrected for instrumental background followed by temperature- and frequency-dependent correction of Raman intensities (Long, 1977). The background correction was carried about by subtracting a spline function fitted through spectral regions without Raman signals from the raw Raman spectra. Segments of the spectral range of the resulting temperature-, frequency-, and background-corrected Raman spectra were fitted to Gaussian lines by using the commercial software package IGOR™ from Wavemetrics.

The Raman spectra were used to characterize speciation of volatiles and of silicate components in melts and fluids and also to determine fluid/melt partition coefficients. Partition coefficients could be determined in this manner because for the same vibration of the same bond in the same structural species in coexisting fluid and melt, the Raman cross-section is the same in spectra of coexisting fluid and melt. These cancel out in a ratio of integrated Raman intensities. The partition coefficient then is the ratio of integrated areas of the Raman signals assigned to given vibration,

$$K_{M-X}^{fluid/melt} = \frac{A_{\nu(M-X)}^{fluid}}{A_{\nu(M-X)}^{melt}}. \quad (1)$$

In this expression, $\nu_{M\text{-}X}$ refers to the vibration of the M-X species of interest and A the integrated area of the Raman band in the spectra of coexisting fluid and melt.

This is a preprint, the final version is subject to change, of the American Mineralogist (MSA)
Cite as Authors (Year) Title. American Mineralogist, in press.
(DOI will not work until issue is live.) DOI: http://dx.doi.org/10.2138/am.2014.4575 



The D/H ratios in individual species in coexisting fluids and melts were determined by using the same principles. To determine D/H ratio, it is also assumed that the Raman cross-sections of D- and H-containing species are the same. In a recent study of D/H partitioning between silicate melt and aqueous fluid in a similar system, Mysen (2013b) found this to be so within the errors associated with determination of area ratios (typically 5-10 % relative to actual value).

*Equilibrium Considerations*

Platinum and molybdenum can serve to enhance isotopic (and chemical) equilibration rates. For example, Horita (1988) found that D/H equilibrium between $H_2O$ and $D_2O$ at 25°C is reached in 1-2 hours in the presence of metallic Pt. In the current experiments at much higher temperature, the samples remained at each temperature for more than 1 hour. Further, previous time studies during *in-situ* experiments with NA10+$H_2O$+$D_2O$ in similar temperature and pressure ranges indicated that D/H equilibrium was reached in minutes (Mysen, 2013b). We conclude, therefore, that equilibrium was reached in the present experiments.

**Results**

The temperature paths were similar for the two series of experiments (Fig. 1). The pressures during the experiment under oxidizing conditions were 30 - >100% higher than those under reducing conditions. The different pressure paths reflect different proportions of fluid and melt, different fluid proportions, and different types of fluid species.

This is a preprint, the final version is subject to change, of the American Mineralogist (MSA)
Cite as Authors (Year) Title. American Mineralogist, in press.
(DOI will not work until issue is live.) DOI: http://dx.doi.org/10.2138/am.2014.4575 



194 *Raman Spectra*

195 The low-frequency region, below about 1200 $cm^{-1}$, comprises signals from the structural
196 environments of silicate components (Fig. 2). In the frequency range between ~2000 and
197 ~2800 $cm^{-1}$, in addition to second-order diamond vibrations from the diamond in the
198 diamond cell, this is where Raman bands from pure $N_2$ and deuterated nitrogen
199 complexes would be found (Fig. 3). The 2800-4200 $cm^{-1}$ range comprises bands assigned
200 to N-H and C-H stretching together with O-H and H-H stretching (Fig. 4).
201
202 Below 1200 $cm^{-1}$. At 800°C and 2165 MPa under oxidizing conditions the spectrum of
203 fluid below 1200 $cm^{-1}$ characteristically shows a strong band near 780 $cm^{-1}$ and a weaker
204 band near 600 $cm^{-1}$ (Fig. 2). There may also be slight intensity above 780 $cm^{-1}$, but this
205 cannot be observed at any temperature less than 800°C. The intensity of both bands
206 diminishes rapidly with decreasing temperature and pressure. These features resemble
207 those of silicate-saturated fluids in hydrous alkali aluminosilicate, silicate, and silica
208 systems under similar pressure and temperature conditions (Zotov and Keppler, 2000;
209 Mibe et al., 2008; Mysen, 2010). The band near 600 $cm^{-1}$ is a bending vibration involving
210 bridging oxygen thus implying silicate polymerization. It follows that the silicate species
211 are dominantly of $Q^0$ and $Q^1$ type at least at the highest temperature and pressure. At
212 lower temperatures and pressures, there is no evidence for silicate species that are more
213 polymerized than $Q^o$.
214 The spectra of fluid under reducing conditions (Mo-$MoO_2$) differ from those of
215 oxidized fluids in that there are additional strong bands centered near 880 and 920 $cm^{-1}$
216 (Fig. 2). The 780 $cm^{-1}$ band, present in spectra of oxidized fluids, remains, but no Raman

 



intensity can be seen at lower frequencies. The 880 and 920 $cm^{-1}$ bands probably cannot be assigned to vibrations associated with silicate (e.g, Si-OH or Si-OD, with symmetric stretching resulting in Raman intensity near 900-970 $cm^{-1}$; see also Stolen and Walrafen, 1976; McMillan and Holloway, 1987) because there is no Raman intensity in this frequency region in the spectra recorded under oxidizing conditions even thought $H_2O$ was also a major component on those experiments. Rather, these bands should be assigned to vibrations involving reduced nitrogen, such as, for example, $Si\text{-}NH_2$ stretching. Such Raman bands occur in this frequency region (Ishida et al., 1982; Dillon et al., 1991).

The absence of Raman bands below 780 $cm^{-1}$ likely means that there are no silicate species with bridging oxygen because that would result in Raman intensity between about 550 and 700 $cm^{-1}$ (Si-O-Si bending; see, for example, Furukawa et al., 1981; Hemley et al., 1987). In other words, the silicate dissolved in fluid under reducing conditions exists only as completely depolymerized $Q^0$ species even at the highest temperatures and pressures used in the illustration of Raman spectra of fluid in Fig. 2.

The Raman spectra of melt are significantly more complex than those of fluids whether under oxidizing or reducing conditions (Fig. 2). There are Raman bands centered near 500, 570, and 600 $cm^{-1}$. Under oxidizing conditions, the spectra show a strong band at and above 780 $cm^{-1}$. The three lowest frequency bands are assigned to rocking and bending motions in Si-O bonding in polymerized silicate structures (Matson et al., 1986; McMillan et al., 1992). The 780 $cm^{-1}$ band is assigned to $Si\text{-}O^-$ stretching in $Q^o$ as for other samples, whereas the broad and strong maximum near 850 and additional bands toward higher frequency (900 $cm^{-1}$ and higher) in spectra of melts recorded under

This is a preprint, the final version is subject to change, of the American Mineralogist (MSA)
Cite as Authors (Year) Title. American Mineralogist, in press.
(DOI will not work until issue is live.) DOI: http://dx.doi.org/10.2138/am.2014.4575 



oxidizing conditions are assigned to stretch vibrations of Si-O bonds in increasingly polymerized silicate species as the frequency increases (e.g., Furukawa et al., 1981; Mysen et al., 1982 McMillan et al., 1992). The intensity in this spectral region of melts under reducing conditions differs from those of melts formed from oxidizing conditions. The bands are narrower, with a maximum near 880 $cm^{-1}$ and a shoulder near 920 $cm^{-1}$. These frequencies are nearly identical to those of the spectra of fluid under reducing conditions. It is probable, therefore, that the structural features that give rise to these intensities in coexisting fluids and melts formed under reducing conditions may resemble one another

2000-2800 $cm^{-1}$. This is the spectral range where Raman bands occur that are assigned to N-D, OD, and N-N vibrations (Loutellier and Perchard, 1989; Walrafen et al., 1996; Schäfer et al., 2012). These could be from molecular $N_2$, from $ND_2$, NHD and OD groups. However, this is also spectral range where the 2.-order Raman spectrum of diamond from the diamond cell itself occurs. This is a very intense group of bands (Fig. 3). This diamond signal imposes, therefore, a strong and complex background on spectra of the fluids and melts. Two examples with fluid under oxidizing and reducing conditions at the highest temperature (800°C) are shown in Fig. 3. Spectra recorded at lower temperature and pressure show the same features.

The spectral range where bands assigned to OD vibrations from $D_2O$ would be expected (e.g., Walrafen et al., 1996) is indicated with double arrows in Fig. 3. The presence of molecular $N_2$ is manifested by a Fermi doublet 2300 $cm^{-1}$ (e.g., Loutellier and Perchard, 1989). These can be seen as sharp peaks in spectra of fluids under both

This is a preprint, the final version is subject to change, of the American Mineralogist (MSA)
Cite as Authors (Year) Title. American Mineralogist, in press.
(DOI will not work until issue is live.) DOI: http://dx.doi.org/10.2138/am.2014.4575 



oxidizing and reducing conditions (Fig. 3). They are weak or cannot be detected in spectra of melts. Deuterium-substituted (N-D)-complexes would be indicated by Raman bands assigned N-D stretching around 2400 $cm^{-1}$ (Schäfer et al., 2012). These positions are marked by arrows in Fig. 3B. However, whether or not these are present cannot be discerned above the strong intensity from the 2.-order diamond intensity in this frequency region.

2800-4200 $cm^{-1}$. The most intense feature in this region, observed in all spectra, is the broad (>100 $cm^{-1}$) slightly asymmetric band centered near 3600 $cm^{-1}$ (Fig. 4). This band – actually a composite of several Raman bands – resembles that reported for water-saturated Na-silicate and aluminosilicate melt+fluid systems (Mysen, 2009, 2010) as well as that of pure $H_2O$ (Walrafen et al., 1986; Frantz et al., 1993). These Raman bands are assigned to O-H stretching in OH-groups in $H_2O$ and HDO (Walrafen et al., 1986; Veirs and Rosenblatt, 1987; Frantz et al., 1993).

There are two groups of bands below the 3600 $cm^{-1}$ maximum in spectra of melts and fluids formed under reducing conditions. There is an asymmetric band near 3320 $cm^{-1}$ with a shoulder near 3350 $cm^{-1}$ (Fig. 4). In spectra of fluids, these can be separated into two distinct bands, whereas in spectra of melts, the bands are so weak that separation into two bands is not statistically meaningful (see also Fig. 4). These bands are assigned to N-H stretching in amine groups ($NH_2^-$) and likely ammonia ($NH_3$) (Yeo and Ford, 1994; Kowal, 2002). Ammonium ($NH_4^+$) groups are unlikely because the N-H stretch bands for $NH_4^+$ groups are between 3000 and 3200 $cm^{-1}$ (Socrates, 2001). Mysen et al. (2008)

 



noted that in Raman spectra of ammonium salts, there were no Raman bands at frequencies greater than 3200 $cm^{-1}$.

In Raman spectra of melts and fluids equilibrated under reducing conditions there is also a doublet of bands near 2920 and 2960 $cm^{-1}$. These bands do not exist in spectra of samples equilibrated under oxidizing conditions (Fig. 4). Their assignment is somewhat complex. One possibility is N-H stretching in $NH_2^+$ functional groups, which would result in a Raman band near 2960 $cm^{-1}$ (Socrates, 2001). However, this interpretation does not explain the 2920 $cm^{-1}$ band. The band cannot be assigned to N-D stretching in $ND_2^-$ or NHD complexes because such a Raman band would occur near 2500 $cm^{-1}$ (Schäfer et al., 2012). It seems, therefore, that the two bands in this doublet should not be assigned to vibrations in N-bearing functional groups. A band near 2920 $cm^{-1}$ has been reported, however, in high-temperature/-pressure *in-situ* Raman spectra of nominally pure $H_2O$ in the hydrothermal diamond anvil cell. A Raman band near 2900 $cm^{-1}$ was originally ascribed to $CH_4$ formed by interaction between $H_2O$ and carbon from the diamond in the diamond cell itself to form $CH_4$ (Chou and Anderson, 2009). Mysen and Yamashita (2010) noted, however, that a more likely source of the carbon is from incomplete cleaning of gaskets after polishing (held in place by Crystal Bond™, an organic adhesive) and/or incomplete removal of organic solvents (acetone) during the same processes. This possibility certainly also exists in the present experiments. If so, the band near 2920 $cm^{-1}$ could be assigned to C-H stretching in $CH_4$ or methyl ($CH_3$) groups and the 2960 $cm^{-1}$ band to C-H stretching in $CH_xD_y$ isotopologues as has been reported in spectra of high-temperature/-pressure $H_2O$-$D_2O$-$CH_4$ fluids (Foustoukos and Mysen, 2013). The frequencies of the bands from the present study are identical, within

 



uncertainty, to those in that study (Fig. 5). The isotopologues were formed by D/H exchange between $CH_4$ and $D_2O$ in the fluid.

Spectra of fluids and melts formed under reducing conditions at the highest temperature and pressure have a weak band near 4140 $cm^{-1}$ (see insert in Fig. 4), which is not observed in spectra of fluids and melts formed under oxidizing conditions. This band has a frequency and a width similar to those of the peak arising from H-H vibration in molecular $H_2$ in $H_2$-saturated $NaAlSi_3O_8$ melts (e.g., Luth et al., 1987).

## Discussion

The band near 2920 $cm^{-1}$ was assigned to C-H stretching in $CH_4$ or methyl ($CH_3$) groups and the 2960 $cm^{-1}$ band to C-H stretching in $CH_xD_y$ isotopologues. There are multiple $CH_xD_y$ isotopologues from which C-H stretching will be slightly different (Foustoukos and Mysen, 2013). However, these the frequency of these individual bands is quite close together and with such extensive overlap at high temperature the individual Raman bands cannot be separated in the spectra. So only two bands are considered. These are also compared with a spectrum of fluid from the system $H_2O$-$D_2O$-$CH_4$-$CD_4$ recorded *in-situ* at 600°C/1053 MPa (Fig. 5). The essentially identical frequencies of the two bands (within spectrometer uncertainty; 3-4 $cm^{-1}$) lends further support to these being assigned to symmetric C-H of in $CH_4$ and $CH_xD_y$ groups in the fluid and melt. From the intensity ratio of these two bands we calculate the abundance ratio of $CH_4$ relative to the group of $CH_xD_y$ isotopologues reflected in the 2960 $cm^{-1}$ band, $A_{2920}/A_{2960}$, in fluid and coexisting melt. This abundance ratio is temperature-dependent and approaches 1 with increasing temperature (Fig. 6). The rate of change, however, differs for melt and fluid. In this

 



regard, these data resemble the temperature-dependent D/H behavior in coexisting aqueous fluid and water-saturated silicate melts (Mysen, 2013b). In this latter case, silicate-speciation considered the controlling factor for the D/H evolution in fluids and melts. Furthermore, in a study methane-saturated melt quenched to a glass from melts equilibrated with $CH_4$+$H_2O$+$H_2$ fluid at similar pressures and temperature carbon isotope fractionation was found significantly dependent on melt compositions (Mysen et al., 2009). Carbon-13 MAS NMR data of these melts indicate that $CH_3$ (methyl) and $CH_4$ (molecular methane) coexist in melt in equilibrium with a $CH_4$+$H_2O$+$H_2$ fluid. The proportion of those functional groups in melts were composition- and temperature-dependent. Carbon isotope fractionation was considered driven, therefore, by these structural effects (Mysen, 2012). It is considered reasonable to assume that both species coexist even though the Raman spectra of the fluids and melts in the present system are insufficiently well resolved to distinguish between methyl groups and methane. These features could explain the temperature-dependent isotope ratios in fluids in melts (Fig. 6).

The different temperature-dependent D/H evolution in fluids and melts leads to the D/H partitioning between (C-O-H-D-N)-saturated melt and silicate-saturated (C-O-H-D-N) fluid (Fig. 7). The $\Delta$H-value is several times higher (33±6 kJ/mol) in the present system than in the simpler (O-H-D)-saturated melt + silicate-saturated (O-H-D) fluid ($\Delta$H=6.5±0.7 kJ/mol) (Mysen, 2013b). The temperature-dependence in Fig. 7 incorporates different (D,H)-bearing species, changes in pressure (from 387 to 843 MPa in the 500°-800°C temperature range of Fig. 7), changes in silicate speciation in the C-O-H-N fluid, and changes in the (C-O-H-N)-saturated silicate melt with temperature and

 



353 pressure. These factors likely account for the different ΔH-values in Fig. 7 compared
354 with those of Mysen (2013b).

355 The nitrogen speciation in oxidized and reduced fluids and melts differs greatly.
356 Nitrogen solubility in silicate melts also varies by more than a factor of 2 depending on
357 nitrogen oxidation state. Reduced nitrogen is the most soluble (Mysen et al., 2008; Kadik
358 et al., 2013). Under oxidizing conditions, there is spectroscopic evidence for $N_2$ in
359 molecular form only in fluid and melt (Fig. 3). Other possible forms of oxidized nitrogen,
360 whether in the form of a nitrosyl group or as nitrate, cannot be discerned as the strongest
361 Raman bands from such groups are near 2100 and 1050 $cm^{-1}$, respectively (Kloprogge et
362 al., 2002; Roskosz et al., 2006). There is no evidence for new Raman bands in these
363 regions of the spectra of fluid and melt formed under oxidizing conditions.

364 The speciation of reduced nitrogen comprises (N-H)-bearing functional groups. The
365 two bands near 3300-3350 $cm^{-1}$ (Fig. 4) likely is because there exist two types of N-H
366 groups, as molecular $NH_3$ and as ammine groups, $NH_2$ (Yeo and Ford, 1994; Kowal,
367 2002; Mysen et al., 2008). In a study of quenched nitrogen-saturated quenched $Na_2Si_4O_9$
368 – N-O-H melt equilibrated with N-O-H fluid under reducing conditions at 1.5
369 GPa/1400°C Mysen et al. (2008) suggested that these groups are associated with Si. This
370 suggestion is also supported by the bands near 880 and 920 $cm^{-1}$, respectively (Figs. 3
371 and 8). In a study of amino-coupled silane this frequency range, Ishida et al. (1982) also
372 suggested that Raman bands in this this frequency range should be assigned to vibrations
373 in Si-$NH_2$ and Si-$NH_3$. As also noted above, an alternative assignment may be to SI-OH
374 stretching as these vibrations can also result in Raman bands >900 $cm^{-1}$ (Stolen and
375 Walrafen, 1976; McMillan and Holloway, 1987). However, if this assignment is correct,

This is a preprint, the final version is subject to change, of the American Mineralogist (MSA)
Cite as Authors (Year) Title. American Mineralogist, in press.
(DOI will not work until issue is live.) DOI: http://dx.doi.org/10.2138/am.2014.4575 



one would also expect Raman bands in this region in spectra of melts equilibrated under oxidizing conditions. However, no such band can be observed.

The principal equilibrium between the two (N+H)-species and the silicate components silicate melts is (Mysen et al., 2008);

$$Q^{n-1}(NH_2) + Q^{n-1}(OH) = 2Q^n + NH_3 \quad (2)$$

We suggest a similar solution mechanism for the ($NH_3$-$NH_2$-$H_2O$-$H_2$)-bearing fluid phase in equilibrium with silicate melt because silicate components in water-bearing fluids in equilibrium with sodium aluminosilicate melts can reach several mol % under the conditions of these experiments. In eqn. (2) the superscript *n* denotes the number of bridging oxygen in the Q-species, $Q^{n-1}(NH_2)$ indicates a Q-species where an oxygen bridge is replaced by an ammine group ($NH_2$) and $Q^{n-1}(OH)$ a Q-species where an oxygen bridge has been replaced by an OH group. In other words, solution of reduced nitrogen, $NH_3$, in silicate melts to form Si-$NH_2$ bonding results in depolymerization of the silicate melt structure.

With the assumption that the Si-$NH_2$ and Si-$NH_3$ vibrations assigned to the 880 and 920 $cm^{-1}$ Raman bands have similar force constants, the ratio of integrated areas of these bands, $A_{880}$ and $A_{920}$, equals the ratio of mol fraction of these species,

$$X_{SiNH3}/X_{SiNH2} = A_{880}/A_{920}. \quad (3)$$

This is a preprint, the final version is subject to change, of the American Mineralogist (MSA)
Cite as Authors (Year) Title. American Mineralogist, in press.
(DOI will not work until issue is live.) DOI: http://dx.doi.org/10.2138/am.2014.4575 



Notably the $NH_2/NH_3$ ratio in fluid is much more sensitive to temperature (and pressure) than in melt (Fig. 8). In other words, the equilibrium constant for equilibrium (2);

$$K = \frac{(Q^n)^2 \bullet X_{NH_3}}{Q^{n-1}(NH_2) \bullet Q^{n-1}(OH)}, \quad (4)$$

shifts to the right with temperature and pressure perhaps because the abundance of hydroxylated silicate, $Q^{n-1}(OH)$, increases with increasing pressure. The greater temperature-sensitivity of equilibrium (2) in fluid likely is because the overall abundance of silicate in the fluid is also temperature and pressure-dependent (Zhang and Frantz, 2000; Newton and Manning, 2003).

In addition to the two bands in the 3300-3350 $cm^{-1}$ range, there is an additional band near 3300 $cm^{-1}$ in the 425° - 650°C temperature range. This band likely is because of hydrogen bonding in the $NH_3$ or $NH_2^-$ groups, or both (Fig. 9; see also Yeo and Ford, 1994).

The Raman spectra of fluids and melts equilibrated under reducing conditions are interpreted to be consistent with similar (N-H) species in both phases (molecular $NH_3$ and $NH_2$-groups forming bonds with $Si^{4+}$). The relationship between integrated areas of Raman bands and mol fraction of coexisting species [eqn. (1)] can, therefore be used to extract fluid/melt partition coefficients for the total (N+H)-species ($NH_2^-+NH_3$) (Fig. 11). Its temperature-dependence yields $\Delta H=45\pm12$ kJ/mol. This treatment is, however, an oversimplification because pressure increases with temperature (Fig.1) and the solubility of reduced nitrogen species in silicate melts is positively correlated with pressure (Mysen

 



et al., 2008). The fluid/melt partition coefficients in Fig. 11 are, therefore, maximum values. The ΔH-value is also a maximum.

**Applications**

The pressure-/temperature-dependence of fluid/melt partition coefficients imply that degassing of N-bearing magmatic liquids in the earth's interior is more efficient the lower the temperature pressure (shallower depth). Furthermore, the degassing process also depends on redox conditions because nitrogen solubility in melts depends on the redox sate of nitrogen (Mysen et al., 2008). The solubility of oxidized nitrogen in silicate melts of similar composition and at the same pressure and temperature is less than 50% of that of reduced N-O-H species (Mysen et al., 2008). This means that fluid/melt partition coefficients most be at least 100% greater for oxidized nitrogen than for reduced nitrogen. It follows from this conclusion that the extent to which nitrogen will be scavenged from the earth's interior is also redox dependent. Nitrogen may not, for example, be treated in a manner analogous to noble gases, where solubility behavior and depletion are simply functions of atomic/molecular ratio. Furthermore, given that nitrogen isotope partitioning between fluids and melts under reducing conditions is melt composition and (N-H)-speciation dependent (Mysen and Fogel, 2010), the redox conditions during melting and degassing of the Earth's interior must take redox conditions into considerations.

**Acknowledgments**

This research was conducted while BOM visited Tohoku University, JAPAN, in 2012 as a visiting professor in $GI^3$ Lab (Global Intellectual Incubation and Integration Laboratory) program of WPI-AIMR (WPI-Advanced Institute for Materials Research), Tohoku University. Their hospitality and assistance is greatly appreciated. The research was supported by NSF grant EAR- 1212754

448 **References**
449
450 Bassett, W.A., Shen, A.H., Bucknum, M., and Chou, I. M. (1994) A new diamond anvil
451 cell for hydrothermal studies to 2.5 GPa and from -190 to 1200°C. Reviews of
452 Scientific Instruments, 64, 2340-2345.
453 Bassett, W.A., Wu, T.-C., Chou, I.-M., Haselton, H.T.Jr., Frantz, J., Mysen, B.O., Huang,
454 W.-L., Sharma, S.K., and Schiferl D. (1996) The hydrothermal diamond anvil cell
455 (HDAC) and its applications. In M.D. Dyar, C.A. McCammon, and M.W. Schaefer,
456 Eds., Mineral Spectroscopy: A Tribute to Roger G. Burns, p. 261-272. The
457 Geochemical Society, Houston.
458 Cartigny, P. and Ader, M. (2003) The nitrogen record of crust-mantle interaction and
459 mantle convection from Archean to present; discussion. Earth and Planetary Science
460 Letters, 216, 425-432.
461 Chou, I.-M. and Anderson, A.J. (2009) Diamond dissolution and the production of
462 methane and other carbon-bearing species in hydrothermal diamond anvil cell,
463 Geochimica et Cosmochimica Acta, 73, 6360-6366.
464 Del Gaudio, P., Behrens, H., and Deubener, J. (2007) Viscosity and glass transition
465 temperature of hydrous float glass. Journal of Non-Crystalline Solids, 353, 223-236.
466 Dillon, A. C., P. Gupta, M. B. Robinson, A. S. Bracker, and S. M. George (1991),
467 Ammonia decomposition on silicon surfaces studied using transmission Fourier
468 transform infrared spectroscopy. Journal of Vacuum Science & Technology:
469 Vacuum, Surfaces and Films, 9, 2222-2230.
470 Dingwell, D.B. and Webb, S.L. (1990) Relaxation in silicate melts. European Journal of
471 Mineralogy, 2, 427-449.
472 Foustoukos, D.I. and Mysen, B.O. (2013) Condensed-phase isotope effects on H/D
473 methane isotopologues dissolved in supercritical aqueous solutions. American
474 Mineralogist, in press.
475 Frantz, J.D., Dubessy, J., and Mysen, B. (1993) An optical cell for Raman spectroscopic
476 studies of supercritical fluids and its application to the study of water to 500 °C and
477 2000 bar. Chemical Geology, 106, 9-26.
478 Furukawa, T., Fox, K.E., and White, W.B. (1981) Raman spectroscopic investigation of
479 the structure of silicate glasses. III. Raman intensities and structural units in sodium
480 silicate glasses. Journal of Chemical Physics, 75, 3226-3237.
481 Hemley, R. J., J. D. Kubicki, and H. K. Mao (1987). In-situ, high-pressure Raman
482 spectroscopy of $MgSiO_3$, $CaSiO_3$ and $CaMgSi_2O_6$ glasses, EOS, 68, 1456.
483 Holland, H.D. (1984) The Chemical Evolution of the Atmosphere and Oceans, 598 p.
484 Princeton University Press, Princeton, NJ.
485 Holloway, J.R. and Blank, J.G. (1994) Application of experimental results to C-O-H
486 species in natural melts. In M.R. Carroll and J.R. Holloway, Eds., Volatiles in
487 Magmas, 30, p. 187-230, Mineralogical Society of America, Washington, D.C.
488 Horita, J. (1988) Hydrogen isotope analysis of natural waters using an $H_2$-water
489 equilibration method: A special implication to brines. Chemical Geology 72, 89-94.
490 Ishida, H., Chiang, C.-h., and Koenig, J.L. (1982) The structure of aminofunctional silane
491 coupling agents: 1. γ-aminopropyltriethoxysilane and its analogues. Polymer 23,
492 251-257.
493 Kadik, A.A., Kurovskaya, N.A., Ignat'ev, Y.A., Kononkova, N.N., Koltashev, V.V., and

Plotnichenko, V.G. (2011) Influence of oxygen fugacity on the solubility of nitrogen, carbon, and hydrogen in $FeO$-$Na_2O$-$SiO_2$-$Al_2O_3$ melts in equilibrium with metallic iron at 1.5 GPa and 1400°C. Geochemistry International, 49, 429-438.

Kadik, A.A., Litvin, Y.A., Koltashev, V.V., Kryukova, E.B., Plotnichenko, V.G., Tsekhonya, T.I., and Kononkova, N.N. (2013) Solution behavior of reduced N–H–O volatiles in $FeO$–$Na_2O$–$SiO_2$–$Al_2O_3$ melt equilibrated with molten Fe alloy at high pressure and temperature. Physics of the Earth and Planetary Interiors, 214, 14-24.

Kasting, J.F., Eggler, D.H., and Raeburn, S.P. (1993) Mantle redox evolution and the oxidation state of the Archean atmosphere. Journal of Geology, 101, 245-257.

Kessel, R., Ulmer, P., Pettke, T., Schmidt, M.W., and Thompson, A.B. (2004) A novel approach to determine high-pressure high-temperature fluid and melt compositions using diamond-trap experiments. American Mineralogist, 89, 1078-1086.

Kloprogge, J.T., Wharton, D., Hickey, L., and Frost, R.L. (2002) Infrared and Raman study of interlayer anions, $CO_3^{2-}$, $NO_3^-$, $SO_4^{2-}$, and $ClO_4^-$ in Mg/Al-hydrotalcite. American Mineralogist, 87, 623-629.

Knoche, R., Dingwell, D.B., Seifert, F.A., and Webb, S.L. (1994) Non-linear properties of supercooled liquids in the system $Na_2O$-$SiO_2$. Chemical Geology 116, 1-16.

Kowal, T. (2002) Anharmonic, vibrational spectra of hydroxylamine and its $^{15}N$, $^{18}O$, and deuterium substituted analogs. Spectrochimica Acta Part A, 58, 1055-1067.

Long, D. A. (1977), Raman Spectroscopy, 276 pp., McGraw-Hill, New York.

Loutellier, A. and Perchard, J.-P. (1989) Force-field calculations on and the Raman spectra of $NH_nD_{3-n}$ ($0 \le n \le 3$) molecules trapped in solid nitrogen. Journal of Molecular Structure, 198, 51-64.

Luth, R.W., Mysen, B.O., and Virgo, D. (1987) Raman spectroscopic study of the solubility behavior of $H_2$ in the system $Na_2O$-$Al_2O_3$-$SiO_2$-$H_2$. American Mineralogist, 72, 481-486.

Luth, R.W., Virgo, D., Boyd, F.R., and Wood, B.J. (1990) Ferric iron in mantle-derived garnets. Implications for thermobarometry and for the oxidation state of the mantle. Contributions to Mineralogy and Petrology, 104, 56-72.

Matson, D.W., Sharma, S.K., and Philpotts, J.A. (1986) Raman spectra of some tectosilicates and glasses along the orthoclase-anorthite and nepheline-anorthite joins. American Mineralogist, 71, 694-704.

McMillan, P. F., and J. R. Holloway (1987), Water solubility in aluminosilicate melts, Contributions to Mineralogy and Petrologym *97*, 320-332.

McMillan, P.F., Wolf, G.H., and Poe, B.T. (1992) Vibrational spectroscopy of silicate liquids and glasses. Chemical Geology, 96, 351-366.

Mibe, K., Chou, I.-M., and Bassett, W.A. (2008) In situ Raman spectroscopic investigation of the structure of subduction-zone fluids. Journal of Geophysical Research, 113, B04208, doi:10.1029/2007JB005179.

Moynihan, C.T., Macedo, P.B., Montrose, C.J., Gupta, P.K., DeBolt, M.A., Dill, J.F., Dom, B.E., Drake, P.W., Easteal, A.J., Elterman, P.B., Moeller, R.P., Sasabe, H., and Wilder, J.A. (1976) Structural relaxation in vitreous materials. Annals of the New York Academy of Sciences, 279, 15-35.

Mysen, B.O. (2007) The solution behavior of $H_2O$ in peralkaline aluminosilicate melts at high pressure with implications for properties of hydrous melts. Geochimica et Cosmochimica Acta, 71, 1820-1834.

Mysen, B.O. (2009) Solution mechanisms of silicate in aqueous fluid and $H_2O$ in coexisting silicate melts determined in-situ at high pressure and high temperature. Geochimica et Cosmochimica Acta, 73, 5748-5763.

Mysen, B.O. (2010) Structure of $H_2O$-saturated peralkaline aluminosilicate melt and coexisting aluminosilicate-saturated aqueous fluid determined in-situ to 800°C and ~800 MPa. Geochimica et Cosmochimica Acta, 74, 4123-4139.

Mysen, B.O. (2012) High-pressure and high-temperature titanium solution mechanisms in silicate-saturated aqueous fluids and hydrous silicate melts. American Mineralogist, 97, 1241-1251.

Mysen, B. O. (2013a) Effects of fluid and melt density and structure on high pressure and temperature experimental studies of hydrogen isotope partitioning between coexisting melt and aqueous fluid. American Mineralogist. In Review.

Mysen, B.O. (2013b) Hydrogen isotope fractionation between coexisting hydrous melt and silicate-saturated aqueous fluid: an experimental study in situ at high pressure and temperature. American Mineralogist, 98, 376-386

Mysen, B.O. and Armstrong, L. (2002) Solubility behavior of alkali aluminosilicate components in aqueous fluids and silicate melts at high pressure and temperature. Geochimica et Cosmochimica Acta, 66, 2287-2297.

Mysen, B. O., and M. L. Fogel (2010), Nitrogen and Hydrogen Isotope Compositions and Solubility in Silicate Melts in Equilibrium with Reduced (N+H)-bearing Fluids at High Pressure and Temperature: Effects of Melt Structure. American Mineralogist, 95, 987-999.

Mysen, B.O. and Yamashita, S. (2010) Speciation of reduced C-O-H volatiles in coexisting fluids and silicate melts determined in-situ to ~1.4 GPa and 800°C. Geochimica et Cosmochimica Acta, 74, 4577-4588.

Mysen, B.O., Virgo, D., and Seifert, F.A. (1982) The structure of silicate melts; implications for chemical and physical properties of natural magma. Reviews of Geophysics and Space Physics, 20, 353-383.

Mysen, B.O., Yamashita, S., and Chertkova, N. (2008) Solubility and solution mechanisms of NOH volatiles in silicate melts at high pressure and temperature - amine groups and hydrogen fugacity. American Mineralogist, 93, 1760-1770.

Mysen, B.O., Fogel, M.L., Morrill, P. L., and Cody, G.D. (2009) Solution behavior of reduced C-O-H volatiles in silicate melts at high pressure and temperature. Geochimica et Cosmochimica Acta, 73, 1696-1710.

Mysen, B.O., Kumamoto, K., Cody, G.D., and Fogel, M.L. (2011) Solubility and solution mechanisms of C-O-H volatiles in silicate melt with variable redox conditions and melt composition at upper mantle temperatures and pressures. Geochimica et Cosmochimica Acta, 75, 6183-6199.

Newton, R.C., and Manning, C.E. (2003) Activity coefficient and polymerization of aqueous silica at 800°C, 12 kbar, from solubility measurements on $SiO_2$-buffering mineral assemblages. Contributions to Mineralogy and Petrology, 146, 135-143.

Pascal, M.L. and Anderson, G.M. (1989) Speciation of Al, Si, and K in supercritical solutions: experimental study and interpretation. Geochimica et Cosmochimica Acta, 53, 1843-1855.

Richet, P., and Y. Bottinga (1984), Glass transitions and thermodynamic properties of amorphous $SiO_2$, $NaAlSi_nO_{2n+2}$ and $KAlSi_3O_8$, Geochimica et Cosmochimica Acta,

 



586 48, 453-471.
587 Roskosz, M., Mysen, B.O., and Cody, G.D. (2006) Dual speciation of nitrogen in silicate
588 melts at high pressure and temperature: an experimental study. Geochimica et
589 Cosmochimica Acta, 70, 2902-2918.
590 Saxena, S.K. and Fei, Y. (1987) High pressure and high temperature fluid fugacities.
591 Geochimica et Cosmochimica Acta, 51, 783-791.
592 Schäfer, T., Kandratsenka, A., Vöhringer, P., Schroeder, J., and Schwarzer, D. (2012)
593 Vibrational energy relaxation of the ND-stretching vibration of $NH_2D$ in liquid $NH_3$.
594 Physical Chemistry Chemical Physics, 14, 11651-11656.
595 Schiferl, D., Nicol, M., Zaug, J.M., Sharma, S.K., Cooney, T.F., Wang, S.-Y., Anthony,
596 T.R., and Fleischer, J.F. (1997) The diamond $^{13}C/^{12}C$ isotope Raman pressure sensor
597 system for high-temperature/pressure diamond-anvil cells with reactive samples.
598 Journal of Applied Physics, 82, 3256-3265.
599 Socrates, G. (2001) Infrared and Raman Characteristic Group Frequencies - Tables and
600 Charts, 3rd ed., 347 p., John Wiley & Sons, Noew York.
601 Stolen, R. H., and G. E. Walrafen (1976). Water and its relation to broken bond
602 defects in fused silica, Journal of Chemical Physics, 64, 2623-2631.
603 Tolstikhin, I.N. and Marty, B. (1998) The evolution of terrestrial volatiles: a view from
604 helium, neon, argon and nitrogen isotope modeling. Chemical Geology, 147, 27-52.
605 Ulmer, P. and Luth, R.W. (1991) The graphite-COH fluid equilibrium in P, T, $f_{O2}$ space:
606 An experimental determination to 30 kbar and 1600°C. Contributions to Mineralogy
607 and Petrology, 106, 265-272.
608 Veirs, D.K. and Rosenblatt, G.M. (1987) Raman line positions in molecular hydrogen: $H_2$,
609 HD, HT, $D_2$, DT, and $T_2$. Journal of Molecular Spectroscopy, 121, 401-419.
610 Walrafen, G.E., Fisher, M.R., Hokmabadi, M.S., and Yang, W.H. (1986) Temperature
611 dependence of the low- and high-frequency Raman scattering from liquid water.
612 Journal of Chemical Physics. 85, 6970-6982.
613 Walrafen, G.E., Yang, W.-H., Chu, Y.C., and Hokmabadi, M.S. (1996) Raman OD-
614 stretching overtone spectra from liquid $D_2O$ between 22 and 152 °C. Journal of
615 Physical Chemistry, 100, 1381-1391.
616 Wood, B.J., Bryndzia, L.T., and Johnson, K.E. (1990) Mantle oxidation state and its
617 relationship to tectonic environment and fluid speciation. Science, 248, 337-345.
618 Yeo, G.A. and Ford, T.A. (1994) Ab initio molecular orbital calculations of the energetic,
619 structural, vibrational and electronic properties of some hydrogen bonded complexes
620 of water, ammonia and hydroxylamine. Spectrochimica Acta 50A, 5-18.
621 Zhang, Y.-G. and Frantz, J.D. (2000) Enstatite-forsterite-water equilibria at elevated
622 temperatures and pressures. American Mineralogist, 85, 918-925.
623 Zotov, N. and Keppler, H. (2000) In-situ Raman spectra of dissolved silica species in
624 aqueous fluid to 900°C and 14 kbar. American Mineralogist, 85, 600-603.
625
626

This is a preprint, the final version is subject to change, of the American Mineralogist (MSA)
Cite as Authors (Year) Title. American Mineralogist, in press.
(DOI will not work until issue is live.) DOI: http://dx.doi.org/10.2138/am.2014.4575 



## Figure Captions

Fig. 1 – Pressure-temperature trajectories of the two series of experiments (solid squares: oxidized. Solid dots: Reduced (Mo-$MoO_2$ buffer).

Fig. 2 –Raman spectra of coexisting melt (solid line) and fluid (dashed line) in the frequency range if (Si,Al)-O vibrations recorded under reducing and oxidizing conditions and temperatures and pressures as indicated.

Fig. 3 – Examples of Raman spectra in the 2000-2800 $cm^{-1}$ frequency region at 800°C and corresponding pressure as indicated. In left panel, central insert shows the spectrum in diamond in the diamond cell with no sample. Left insert shows the region between 2250 and 2350 $cm^{-1}$ greyed area on main spectrum). On the right spectrum (reducing conditions) is also indicated the approximate frequency of N-D and $D_2O$ vibrations. At lower temperature, the Fermi doublet of $N_2$ between 2250 and 2350 $cm^{-1}$ becomes less intense. It is also less intense in spectra of melt compared with spectra of fluid.

Fig. 4 - Raman spectra of melt (solid line) and coexisting fluid (dashed line) under oxidizing and reducing conditions and at temperatures and pressures as indicated in the 2800-4200 $cm^{-1}$ region. Inserts show expanded view of spectra of fluid under reducing conditions between 2800 and 3400 $cm^{-1}$ and 4100 and 4180 $cm^{-1}$.

Fig. 5 – Example of curve-fitted portion (2800-3050 $cm^{-1}$) of spectrum of melt and fluid at 650°C and 760 MPa recorded under reducing conditions. Also shown is a curve-fitted spectrum in the same frequency region from $H_2O$-$D_2O$-$CH_4$-$CD_4$ supercritical fluid at 600°C/1053 MPa (data from Foustoukos and Mysen, 2013). Note that in these three panels the exact frequencies from the fits are shown. These spectra were recorded with 600 mm/grating groove density, so the frequency uncertainty for each band is 3-4 $cm^{-1}$.

Fig. 6 – Temperature (and pressure – see Fig. 1) variations of the integrated intensity ratio of 2920 relative to2960 $cm^{-1}$ band (mol fraction ratio, $X_{CH4}/X_{CHxDy}$) for coexisting fluid and melt under reducing conditions.

Fig. 7 – Temperature (and pressure - see Fig. 1) dependence of fluid/melt partition coefficient of $CH_4/CH_xY_D$ from the integrated area ratio of the 2920 $cm^{-1}$ and 2960 $cm^{-1}$ Raman bands. See text for additional details.

Fig. 8 – Temperature (and pressure – see Fig. 1) variations of the integrated intensity ratio of 800 relative to 920 $cm^{-1}$ band, considered equal to the abundance ration, $X_{SiNH3}/X_{SiNH2}$, for coexisting fluid and melt under reducing conditions. Inserts show fitted Raman spectra in the relevant frequency regions at temperatures and pressures indicated.

Fig. 9 – Example of curve-fitted portion (3260-3400 $cm^{-1}$) of spectrum of fluid at 575°C and 692 MPa recorded under reducing conditions.

Fig. 10 – Temperature (and pressure - see Fig. 1) dependence of ratios Raman bands assigned to N-H vibrations in fluid under reducing conditions (as illustrated in Fig. 6). Note that the temperature range is limited to that where both Raman bands can be observed in spectra of fluid.

Fig. 11 – Temperature (and pressure - see Fig. 1) dependence of fluid/melt partition coefficient of (N+H)-containing species ($\Sigma NH=NH_2+NH_3$).

 



673 Fig. 12 - Examples of Raman spectra of melt (solid line) and coexisting fluid (dashed
674 line) under oxidizing and reducing conditions as indicated in the 2250-2350 $cm^{-1}$
675 region at 800°C and corresponding pressure as indicated with approximate
676 background from 2nd-order Raman intensity from diamond cell diamond
677 subtracted.

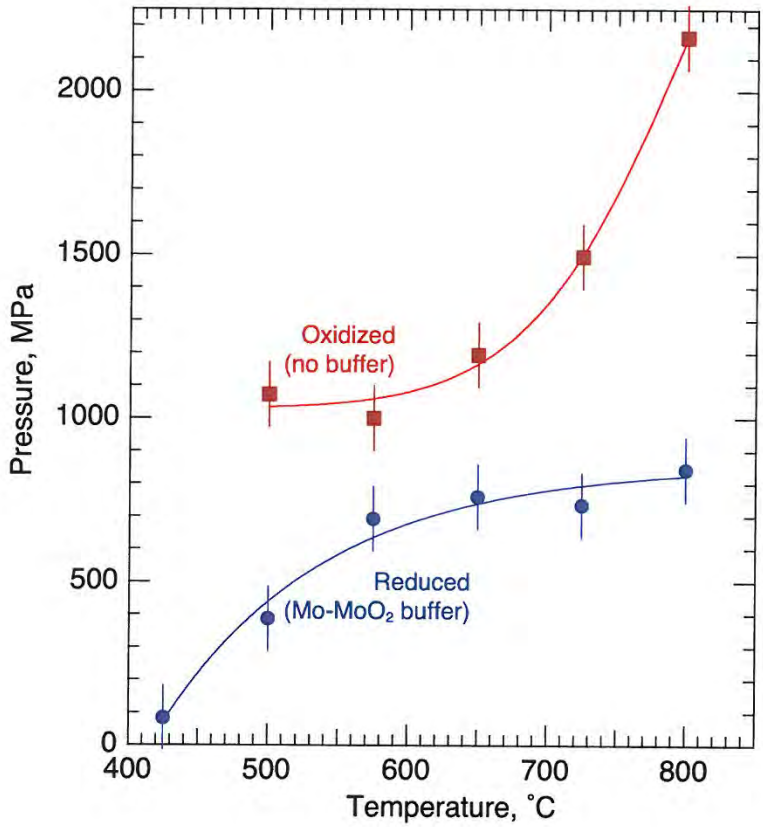
2000
1500
1000
500
0
Pressure, MPa
400
500
600
700
800
Temperature, ˚C
Oxidized
(no buffer)
Reduced
(Mo-MoO2 buffer)

Fig. 1

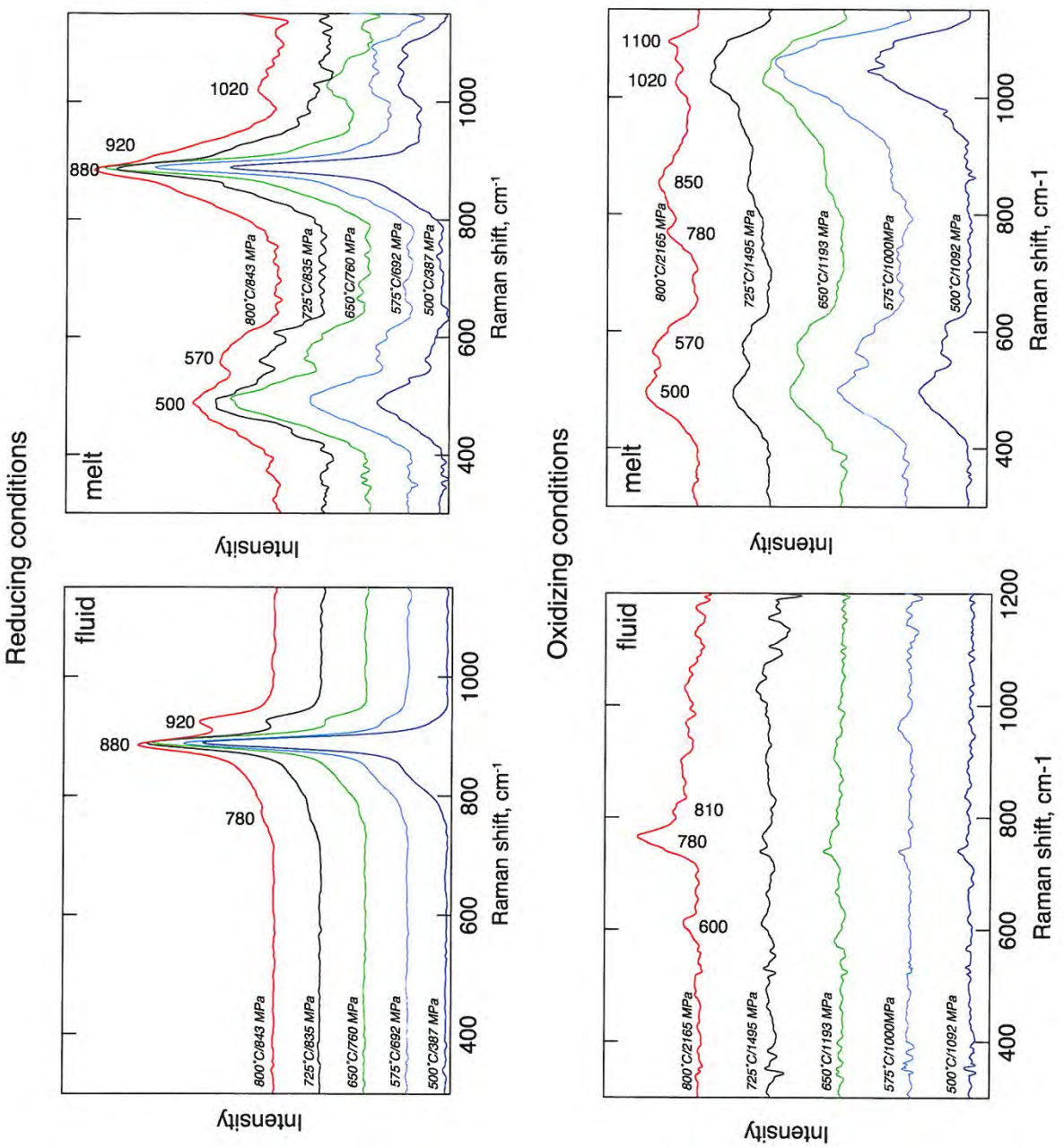
Reducing conditions
melt
fluid
1020
920
880
570
500
780
800°C/843 MPa
725°C/835 MPa
650°C/760 MPa
575°C/692 MPa
500°C/387 MPa
Intensity
Raman shift, cm-1
400
600
800
1000
Oxidizing conditions
1100
850
810
600
800°C/2165 MPa
725°C/1495 MPa
650°C/1193 MPa
575°C/1000MPa
500°C/1092 MPa
1200

Fig. 2

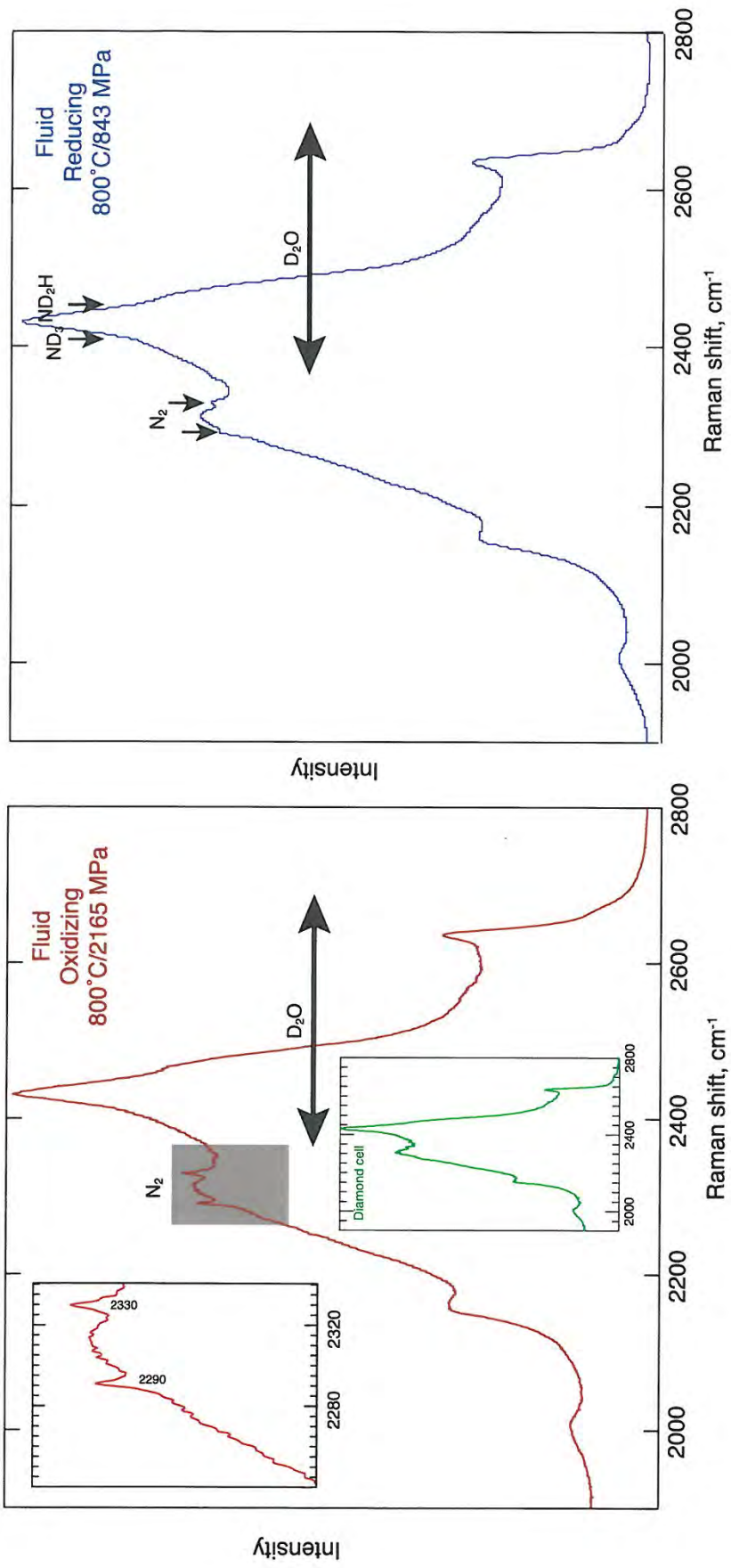
Fluid
Reducing
800°C/843 MPa
$ND_3$
$ND_2H$
$N_2$
$D_2O$
Intensity
2000
2200
2400
2600
2800
Raman shift, cm$^{-1}$
Fluid
Oxidizing
800°C/2165 MPa
$N_2$
$D_2O$
Diamond cell
2330
2290
2280
2320
2000
2400
2800
Intensity
Raman shift, cm$^{-1}$

Fig. 3

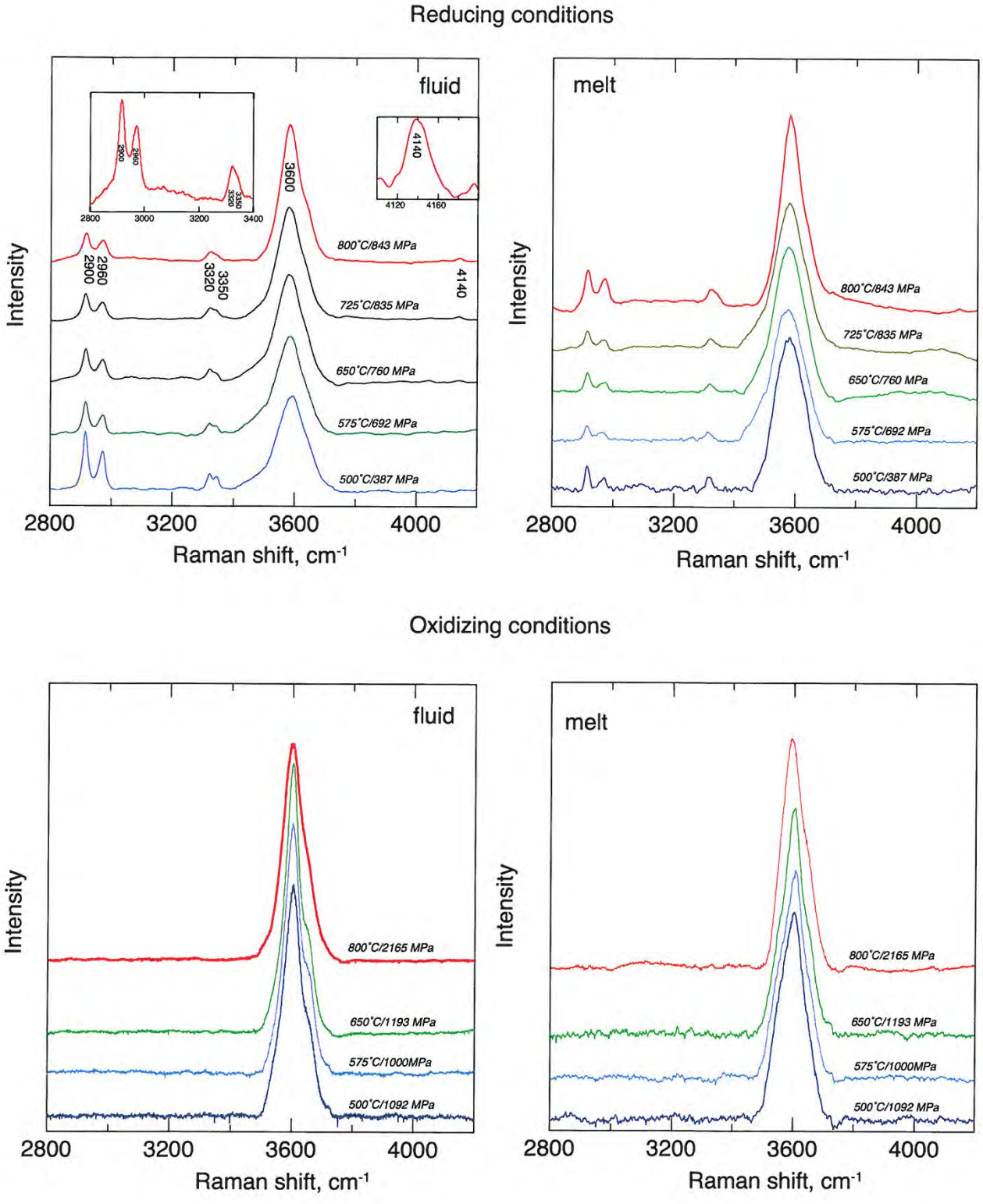
Reducing conditions
fluid
melt
Intensity
2900
2960
3320
3350
3600
4140
800°C/843 MPa
725°C/835 MPa
650°C/760 MPa
575°C/692 MPa
500°C/387 MPa
2800
3200
3600
4000
Raman shift, cm-1
Oxidizing conditions
fluid
melt
Intensity
800°C/2165 MPa
650°C/1193 MPa
575°C/1000MPa
500°C/1092 MPa
2800
3200
3600
4000
Raman shift, cm-1

Fig. 4

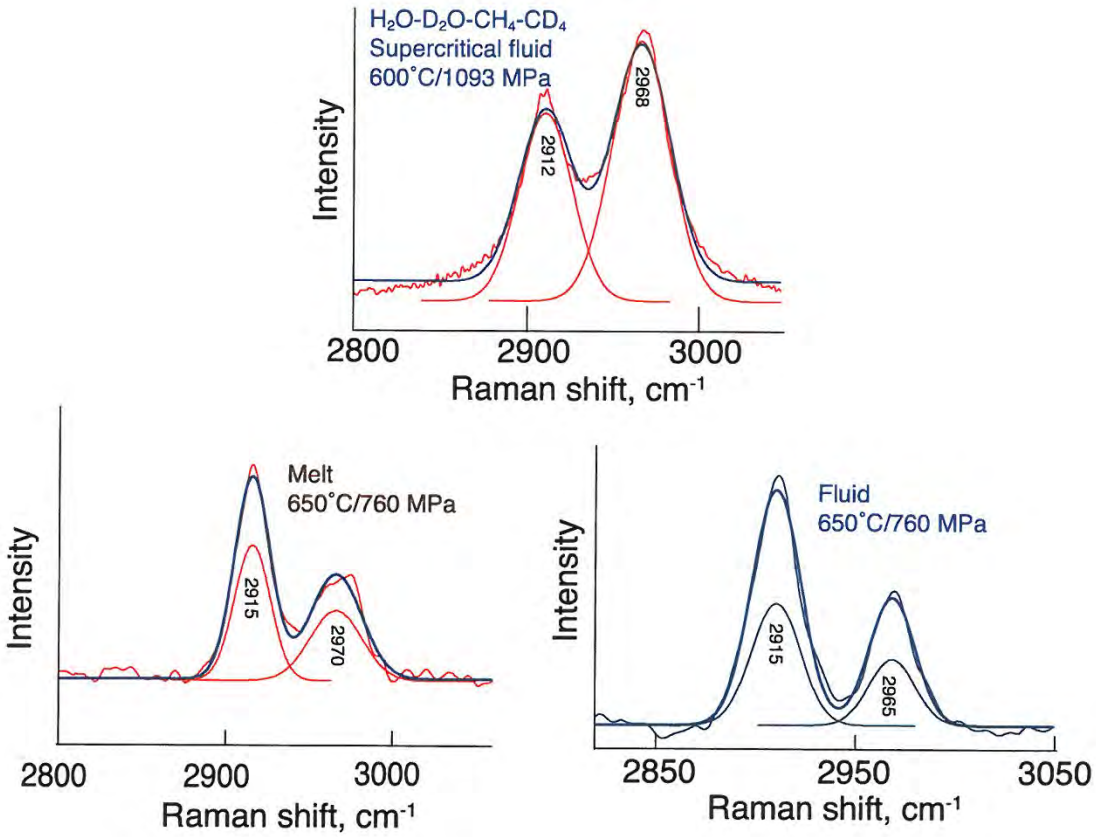
H2O-D2O-CH4-CD4
Supercritical fluid
600˚C/1093 MPa
2912
2968
Intensity
2800
2900
3000
Raman shift, cm-1
Melt
650˚C/760 MPa
2915
2970
Intensity
2800
2900
3000
Raman shift, cm-1
Fluid
650˚C/760 MPa
2915
2965
Intensity
2850
2950
3050
Raman shift, cm-1

Fig. 5

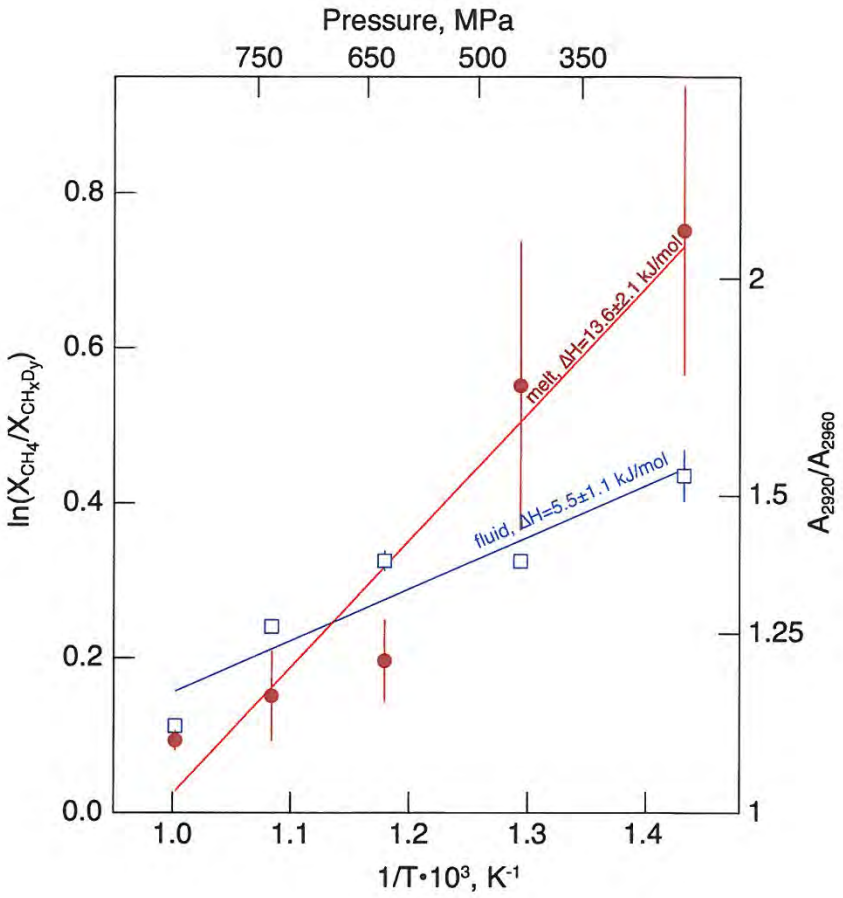
Pressure, MPa
750
650
500
350
0.8
0.6
0.4
0.2
0.0
2
1.5
1.25
1
melt, ΔH=13.6±2.1 kJ/mol
fluid, ΔH=5.5±1.1 kJ/mol
1.0
1.1
1.2
1.3
1.4
1/T•10³, K⁻¹
ln(X_CH4/X_CHxDy)
A2920/A2960

Fig. 6

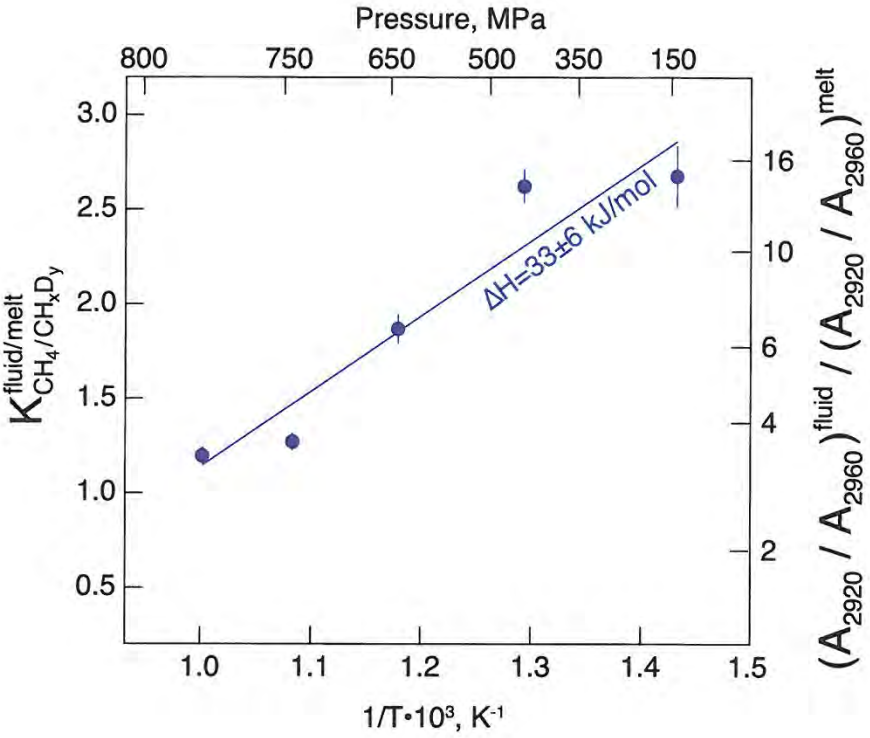
Pressure, MPa
800
750
650
500
350
150
3.0
2.5
2.0
1.5
1.0
0.5
16
10
6
4
2
ΔH=33±6 kJ/mol
$K^{fluid/melt}_{CH_4/CH_xD_y}$
$(A_{2920} / A_{2960})^{fluid} / (A_{2920} / A_{2960})^{melt}$
1.0
1.1
1.2
1.3
1.4
1.5
1/T•10³, K⁻¹

Fig. 7

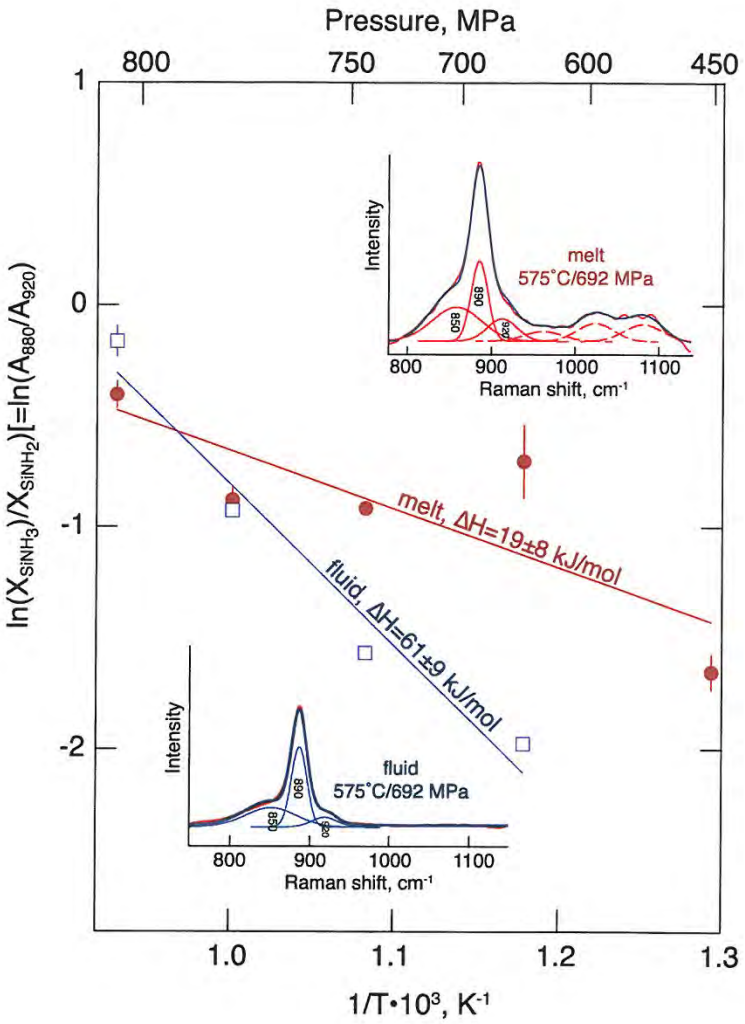
Pressure, MPa
800
750
700
600
450
1
0
-1
-2
ln(X_SiNH3/X_SiNH2)[=ln(A880/A920)]
melt, ΔH=19±8 kJ/mol
fluid, ΔH=61±9 kJ/mol
Intensity
melt
575°C/692 MPa
850
890
920
800
900
1000
1100
Raman shift, cm-1
Intensity
fluid
575°C/692 MPa
850
890
920
800
900
1000
1100
Raman shift, cm-1
1.0
1.1
1.2
1.3
1/T•10³, K-1

Fig. 8

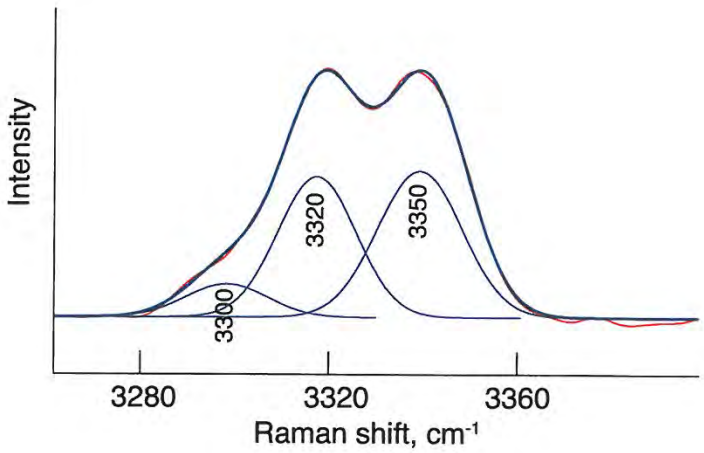


Fig. 9

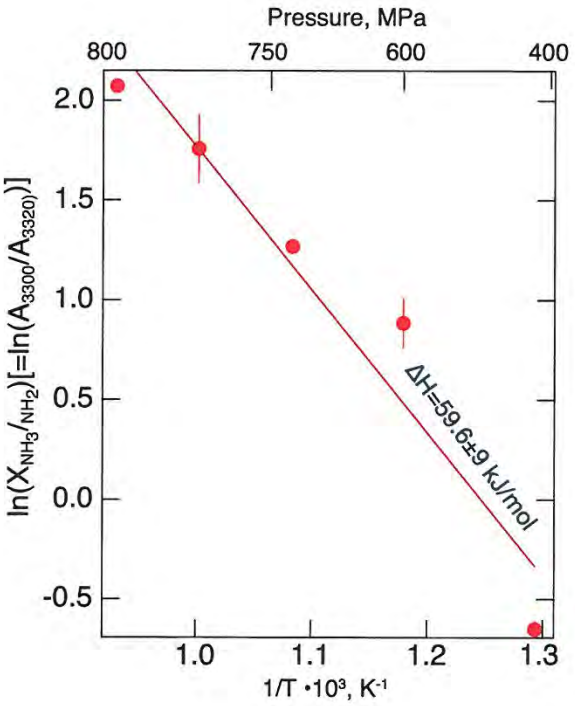
Pressure, MPa
800
750
600
400
2.0
1.5
1.0
0.5
0.0
-0.5
ln(X_NH3/NH2)[=ln(A3300/A3320)]
ΔH=59.6±9 kJ/mol
1.0
1.1
1.2
1.3
1/T •10³, K⁻¹

Fig. 10

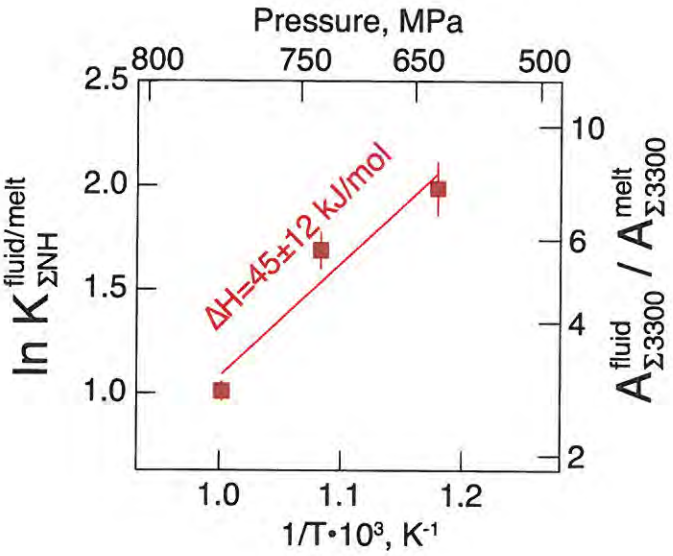
Pressure, MPa
800
750
650
500
2.5
2.0
1.5
1.0
10
6
4
2
1.0
1.1
1.2
1/T•10³, K⁻¹
ln K fluid/melt ΣNH
A fluid Σ3300 / A melt Σ3300
ΔH=45±12 kJ/mol

Fig. 11

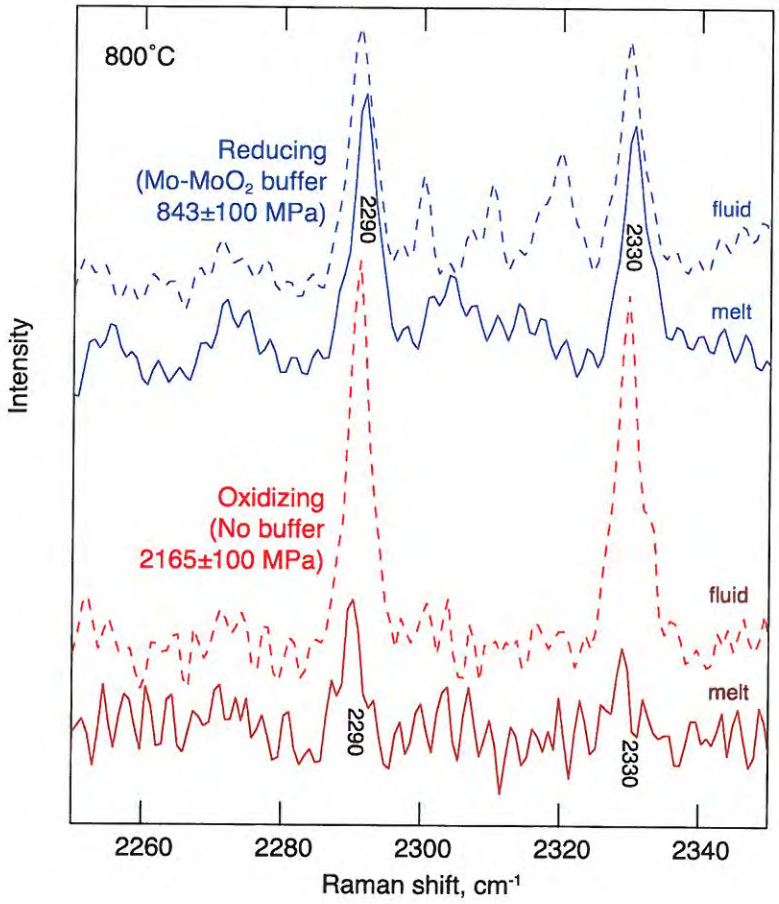
800°C
Reducing
(Mo-MoO2 buffer
843±100 MPa)
2290
2330
fluid
melt
Intensity
Oxidizing
(No buffer
2165±100 MPa)
fluid
melt
2290
2330
2260
2280
2300
2320
2340
Raman shift, cm-1

Fig. 12